Feasibility of hovering small-scale low Reynolds number rotor-beam source localization by microphone array measurements

Hélène Parisot-Dupuis, Romain Gojon, Nicolas Doué, Bertrand Mellot

10.2514/6.2024-3063

Feasibility of hovering small-scale low Reynolds number rotor-beam source localization by microphone array measurements

H. Parisot-Dupuis*, R. Gojon†, N. Doué‡ and B. Mellot§
ISAE-SUPAERO, University of Toulouse, Toulouse, France

The radiation of a small-scale low Reynolds number two-bladed rotor of $0,2\ m$ diameter with NACA0012 blade profile in interaction with cylindrical beams at different locations is measured in anechoic room by an array of 45 microphones. Source localization algorithms are used to localize tonal noise sources associated to blade passing frequency (BPF) harmonics that are increased by the presence of the beam in order to better understand noise source generation mechanisms. A first set of BPF harmonics, consisting of a hump centered around $5 * BPF$, appears to be localized above the rotor near the blade tip, whereas a second set of BPF harmonics, consisting of a hump centered around $20 - 25 * BPF$, seems to have its origin just below the beam in most cases and at $\sim 85\%$ of the blade radius. The increase of rotational speed, beam diameter and the decrease of rotor-beam distance leads to an increase of the first BPF harmonics hump sound levels with similar source locations, except for the noisier rotor-beam configuration for which both humps are located near the blade tip. As this was not consistent with numerical simulations performed on the same configuration which showed that first BPF harmonics levels were associated to unsteady loading on the beam, new simulations were performed to obtain wave fronts between the rotor-beam setup and the array. This allows to explain source locations on maps and to identify which sources were associated to the beam.

I. Nomenclature

BPF	=	blade passing frequency (Hz)
CAA	=	computational aeroacoustics
CBF	=	conventional beamforming
$CLEAN-SC$	=	CLEAN based on spatial source coherence
$CSMDR$	=	cross-spectrum matrix diagonal removal
$DAMAS$	=	deconvolution approach for the mapping of acoustic sources
FFT	=	fast Fourier transform
$FW-H$	=	Ffowcs-Williams and Hawkings
$iLES$	=	implicit large eddy simulations
NF	=	nearfield focusing
φ	=	azimuth angle ($^\circ$)
$PSF's$	=	point spread functions
RPM	=	rotation per minute (min^{-1})
SPL	=	sound pressure level (dB)
SWL	=	sound power level (dB)
θ	=	latitude angle ($^\circ$)
UAV	=	unmanned air vehicles
CFD	=	computational fluid dynamics

*Associate professor, ISAE-SUPAERO, Toulouse, France, helene.parisot-dupuis@isae-supaero.fr, AIAA Member.
†Associate professor, ISAE-SUPAERO, Toulouse, France, romain.gojon@isae-supaero.fr, AIAA Member.
‡Associate professor, ISAE-SUPAERO, Toulouse, France, nicolas.doue@isae-supaero.fr.
§Test engineer, ISAE-SUPAERO, Toulouse, France, bertrand.mellot@isae-supaero.fr.

II. Introduction

With the recent development of unmanned air vehicles (UAVs) for military and civilian applications, small-scale low Reynolds number rotors noise arouses the interest of researchers. Indeed, past studies on rotors operating at high Reynolds number, and mainly dedicated to helicopters [1], are not directly transposable to UAVs. In addition, quadcopter UAVs configurations present complex rotor-rotor and rotor-airframe interactions, generating new sources of noise while being closest to civilian population.

First experimental studies of low Reynolds and low Mach numbers isolated hovering rotors were performed by Zawodny *et al.* [2] in anechoic room, showing that the dominant noise sources were the tonal noise occurring at the blade passing frequency (BPF), which is relatively low for UAVs, and the broadband noise due to the trailing edge flow in the high frequency range. Complementary studies of the noise radiated by low Reynolds number rotors in interaction with airframe components were then performed [3]. They reported hovering anechoic room experiments and numerical simulations of a two-bladed rotor in interaction with a frame, evidencing an increase of the noise radiated, strongly dependent on the frame geometry and location respect to the rotor. More recently, Wu *et al.* [4] proposed analytical models of the unsteady loading of propeller blades and beam, showing directivity patterns in good agreement with both experimental and numerical data. Complementary analytical studies were conducted by Roger *et al.* [5] who addressed both steady and unsteady loading (due to blade-potential interaction) of rotor blades, and cylinder scattering (due to sources compacity). Directivity patterns obtained were also consistent with experimental and numerical results on the studied test case. Gojon *et al.* experimental open database on academic isolated rotors [6] was also recently extended to low Reynolds number rotors in interaction with beams of different shapes and located at different distances from the rotor disk plane. A comparison with measurements performed without beam showed that BPF harmonics levels are increased by the presence of the beam, describing two humps, a first one centered around $5 * BPF$ and a second one centered around $20 * BPF - 25 * BPF$. The levels of the first hump, which is dominant, increase with beam diameter, the rotational speed and the number of blades, but decreases with the rotor-beam distance. Non-compressible implicit large eddy simulations (iLES) associated with a solid Ffowcs-Williams and Hawkings (FW-H) formulation [7] were conducted in complement on one of the experimental configuration. This work was recently extended by Doué *et al.* [8] who used solid FW-H formulation taking into account separately, only the rotor surface, only the beam surface, and only portions of the beam. Results showed that the first hump, centered around $5 * BPF$, was radiated mainly by the beam at $80 - 90\%$ of the blade radius (i.e. near the blade tip), suggesting that the noise mechanism may be related to unsteady loading on the beam.

An interesting way of improving aeroacoustics noise sources understanding, which presents often multiple sources and/or complex interaction phenomenon, is the use of microphone array localization methods. Indeed, such approach allows to discriminate the different sources while providing a ranking of each of them for the frequencies of interest. The most famous source localization algorithm is the conventional beamforming (CBF) method developed by Billinglsey *et al.* [9], which is based on the assumption that the sound field radiated by the sources under study follows a certain source model (uncorrelated monopoles). The principle is to localize the sound sources from farfield microphone array measurements by interpreting the propagation delays measured between each microphone of the array and knowing the source-array distance. As this robust technique presents some drawbacks, advanced methods have been developed to better assess the sound level of the studied sources while improving spatial resolution [10–13]. The problematic of localizing rotating sources was first addressed by Sijstma *et al.* [14], who proposed to use a rotational speed signal associated with a formulation based on convected moving monopoles. This methodology was successfully applied to helicopter [15], turbofan [16] and wind turbine [17] noise studies. Application to small-scale UAVs configurations present some challenges, indeed their small size and low Reynolds number range require an accurate spatial resolution, especially in the low frequency range associated to BPF and its harmonics. Microphone array measurements were recently performed on a small-scale low Reynolds number quadcopter in aeroacoustic wind tunnel by Zawodny *et al.* [18]. In this study CBF allowed to identify rotors self noise and rotor strut-airframe junction interactional noise sources supposed due to the impingement of the upstream airframe and rotor wakes. The efficiency of custom-designed rotors for noise reduction was also assessed.

This paper investigate the feasibility of using microphone array measurements to study a hovering small-scale low Reynolds number rotor noise radiation in interaction with a beam. In the first section the experimental setup used for both directivity and microphone array measurements in anechoic room is presented, as well as the impact of the beam on spectra. The second section is dedicated to the investigation of rotor-beam interaction noise through source localization. The methodology used is first presented, then tonal noise sources at BPF harmonics are identified and their evolution with respect to the different setup parameters is assessed. Finally a complementary numerical study is performed to obtain wave fronts in one configuration in order to better understand the source locations found.

III. Anechoic room measurements

A. Rotor-beam test bench

A two-bladed academic rotor with a NACA0012 blade cross section profile extruded in the radial direction, a constant chord of $0,025\ m$, a constant pitch of 10° and a diameter of $0,2\ m$ is studied. This rotor is located at the top of a test stand at the center of the ISAE-SUPAERO anechoic room, which is acoustically treated in the frequency range $80-16000\ Hz$, and has wedge-tip to wedge-tip dimensions of $5.02*5.24*5.34\ m^3$ ($L*W*H$). Cylindrical beams of different diameters can be positioned at several distances below the rotor disk plane. This distance is defined as the distance between the rotor disk plane, considered as the plane passing through the blades at mid-chord, and the center of the beam. In this experimental campaign, both the rotor and the beam have been 3D-printed using stereolithography.

The rotor is driven by means of a Faulhaber 3274G024BP4 3692 electric brushless motor, which presents low noise emissions and allows precise real-time rotational speed (RPM) control thanks to its associated motion controller MC5010 [19]. The rotational speed of the rotor varies from 6000 to 8000 RPM in the present study. A directivity antenna with 13 1/4 in. GRAS 40PH microphones is used to measure the farfield noise radiated $1.62\ m$ away from the rotor center, for latitude angles θ every 10° from −60° to +60°, where 0° corresponds to the rotor disk plane. Moreover, to be able to study the directivity along the rotor disk plane, the test stand is fixed on a turntable, which can rotate the entire rotor-beam setup in azimuth. With the couple directivity antenna / turntable, the almost complete spherical directivity can be investigated [6]. Additionally a microphone is placed on the nearfield of the rotor, $0.25\ m$ away and $0.25\ m$ below the rotor disk plane. A photograph of the of experimental setup is provided in Fig. 1.

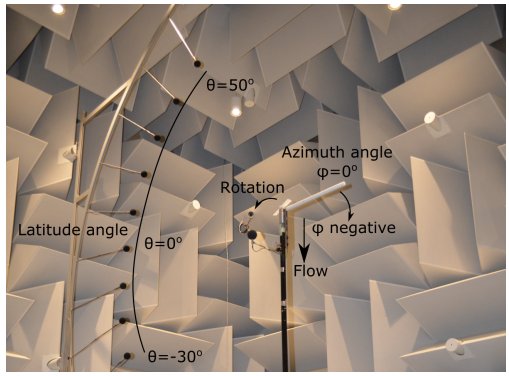

Fig. 1 Photograph of the rotor-beam test bench in ISAE-SUPAERO anechoic room.

B. Microphone array setup

The microphone array used was a LMS Circular Irregular Array of diameter $0,5\ m$ and developed by MicrodB. This 2D array contains a camera with a wide angle lens on its center which allows to take a picture of the source of interest and corrects automatically the picture for the wide angle distorsion. The microphone distribution is composed by 45 1/4 in. GRAS 40PH microphones located on 3 concentric circles with irregular spacing, the smaller being on the internal circle and the larger on the external one. This irregular circular distribution provides an averaged dynamic range, which corresponds to the ratio between the highest and the smallest level that it is possible to distinguish on source maps, around 20 dB for frequencies below 5000 Hz, 12 dB for frequencies between 5000 and 8000 Hz and 7 dB above 8000 Hz for free field monopole radiation. The maximal frequency that can be studied with this antenna is 20000 Hz, the minimal one as well as the spatial resolution depending on the source localization algorithm used.

A cartesian coordinate reference frame with the origin at the center of the rotor is used in the following. The x-axis and y-axis are horizontals and positives in the array and beam directions respectively, whereas the z-axis is vertical pointing upward. The source plane on which source maps will be estimated is defined as the vertical plane (y,z) passing through rotor and beam axis, and the microphone array is positioned parallel to this source plane at a distance of $x = 0.56\ m$. The array center is situated $z = -0.01\ m$ below the rotor disk plane as shown in Fig. 2.

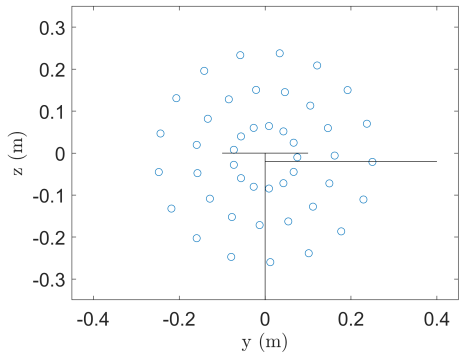

Fig. 2 Microphone array positioning respect to the rotor-beam setup.

C. Effect of the beam on spectra

A previous test campaign, dedicated to the study of the noise generated by the same rotors with various blades numbers in interaction with beams at different distances from the rotor, evidenced that the presence of the beam leads to an increase of BPF harmonics from $2 * BPF$ until $35 * BPF$, leading to a first hump with a maximum level around $5 * BPF$ and a second one centered around $20 * BPF$ [6].

This effect is presented Fig. 3 for the case of the two-bladed rotor rotating at 8000 RPM in interaction with the 0.02 m diameter beam located 0.02 m below the rotor disk plane. Spectra measured at $\varphi = 90°$ and latitude angles $0°$, $-20°$ and $-40°$ on the directivity antenna are compared with the one measured at $-17°$ on the microphone array and transposed to 1.62 m assuming free field spherical decay. This shows that, even if the microphone array is not in the farfield for the whole frequency range, the sound pressure levels (SPL) measured by the microphone array and the directivity antenna are consistent. The spectrum measured on the directivity antenna at $-20°$ without beam is also presented to better highlight the BPF harmonics increase due to the presence of the beam. Dashed lines represent levels of the BPF and its harmonics.

All acoustic data are acquired at a sampling frequency of 51.2 kHz, during 16 s. Spectra presented in this paper are then obtained by computing the fast Fourier transform (FFT) on those signals with a Hanning window applied on 100 segments and a sample overlap of 50%, leading to a frequency resolution of 3.125 Hz.

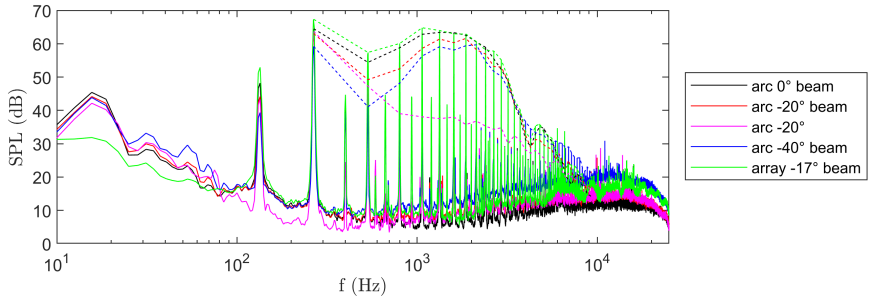

Fig. 3 Sound pressure levels (SPL) measured by directivity antenna ('arc') and microphone array ('array') at 8000 RPM**, different latitude angles &** $\varphi = 90°$ **for the beam of diameter** $0,02$ m **at** $-0,02$ m**. Isolated rotor SPL measured on the directivity antenna for the latitude angle** $-20°$ **is also plotted.**

IV. Investigation of rotor-beam interaction noise by source localization

A previous numerical study [8] showed that the BPF radiation is principally due to rotor radiation, but that the BPF harmonics increase seems to be mainly due to the beam radiation. As this conclusion suggests a noise generation mechanism related to unsteady loading when the blade passes above the beam, the chosen procedure was to try to study this tonal noise component using microphone array measurements parallel to the beam and sound source localization algorithms based on fixed sources (as done recently by Zawodny *et al.* [18]).

A. Algorithm selection

Firstly four existing sound source localisation algorithms are used to study the rotor-beam interaction noise in order to select the more suitable for the following analysis: conventional beamforming (CBF), nearfield focusing (NF), and deconvolution methods (CIRA, CLEAN-SC) [9, 10, 12, 13].

1. Tested algorithms

The conventional beamforming (CBF) [9] is a robust method used as reference in the sound source localization community. However, it has some drawbacks, seldom addressed in the literature, which motivate the development of more advanced methods. A first limit is the low spatial resolution ($\sim \lambda$) in the low-frequency range. A second limit is the presence of side-lobes associated with microphones distribution that can lead to additional wrong sources. This can be limited by using optimized arrays or by removing the diagonal of the array cross-spectrum matrix (CSM DR) during source maps computation. A third limit is that, in the case of multiple sources, the CBF can localize sources but is not able to properly quantify them.

The nearfield focusing (NF) method is a bayesian inference algorithm [13] which uses a statistical approach to solve the sound source localization problem. This method is a very versatile inverse array method as it peforms a regularization of matrix pseudo-inversion, which allows particularly to improve the spatial resolution respect to CBF ($\sim 0.44\lambda$). A particularity of this statistical approach is also the ability to mathematically include a prior information on the solution and to decompose the source field onto geometry-dependent spatial basis functions.

The deconvolution methods principle is to identify the theoretical beam patterns obtained by applying CBF using synthetic microphone data of a single centered monopole source, which corresponds to a kind of array footprint in the source map called point spread functions (PSF's). The objective of deconvolution is to find a way to replace these PSF's by single points in order to remove wrong sources while improving spatial resolution and sources level assessment. Two methods belonging to this family are used in this study.

The algorithm CIRA [10] is a deconvolution methods close to DAMAS [11] in the problem formulation. The principle is to use a steepest gradient descent instead of a Gauss-Seidel procedure to iteratively deconvolute beamforming source maps. This allows to improve the low frequency spatial resolution of beamforming maps while separating several sources from each other and giving a relevant sound power level (SWL) for each one. However, as the deconvolution process is an iterative method, the computational cost increases respect to CBF. A source decorrelation assumption between point sources is made in this algorithm.

The CLEAN-SC algorithm [12] is another deconvolution method based on the CLEAN method used in Astronomy which iteratively removes PSF's of peak sources from a "dirty map". As an uncorrelated monopole source model is used while applying the CBF process [9], CLEAN-SC iteratively removes the part of the source map which is spatially coherent with the main source found by CBF assuming that it is associated to side-lobes. A feature of CLEAN-SC is its ability to estimate absolute sound power levels from the source maps, while improving source maps accuracy with a computational time higher than CBF but lower than CIRA.

2. Algorithms comparison

For the four methods, source maps calculations have been computed from array microphone signals of 15 s with a sample overlap of 50% for FFT in order to have a frequency resolution of 10 Hz. The calculation grid in the source plane is a grid which cells of size of 0.01 m on the range $y = \pm 0.55$ m and $z = \pm 0.4$ m, leading to a total of 9020 points. The CSM DR technique is used for maps averaging computation to obtain a single acoustic map from a time selection including multiple FFT time segments. A dynamic range of 10 dB is used for source maps to facilitate the interpretation. Please note that levels of CBF and NF maps are SPL, whereas the ones of CIRA and CLEAN SC are expressed as SWL due to the iterative deconvolution process which is done on source cross-powers [20].

Sound source maps obtained with the different algorithms on the frequency range from $2 * BPF$ to $35 * BPF$ in the case where the two-bladed rotor is in interaction with a beam of diameter $0,015$ m located $0,025$ m below the rotor disk plane for a rotational speed of 7000 RPM are presented Fig. 4. Locations of the rotor, the beam and the test stand are indicated by lines on the source maps. As expected, the spatial resolution is improved, compared to CBF, for this frequency range including low frequencies ($466 - 8166$ Hz) by using inverse matrix regularization (NF), and even more by using deconvolution (CIRA and CLEAN-SC). The main source appears to be located near the blade tip which is above the beam on the four source maps, but the higher resolution of CIRA maps seems to show two different sources contributions: a first one close to the blade tip and second one close to the beam just below the blade tip. Only a main point source above the blade tip is visible on CLEAN SC map for which the deconvolution process is very selective.

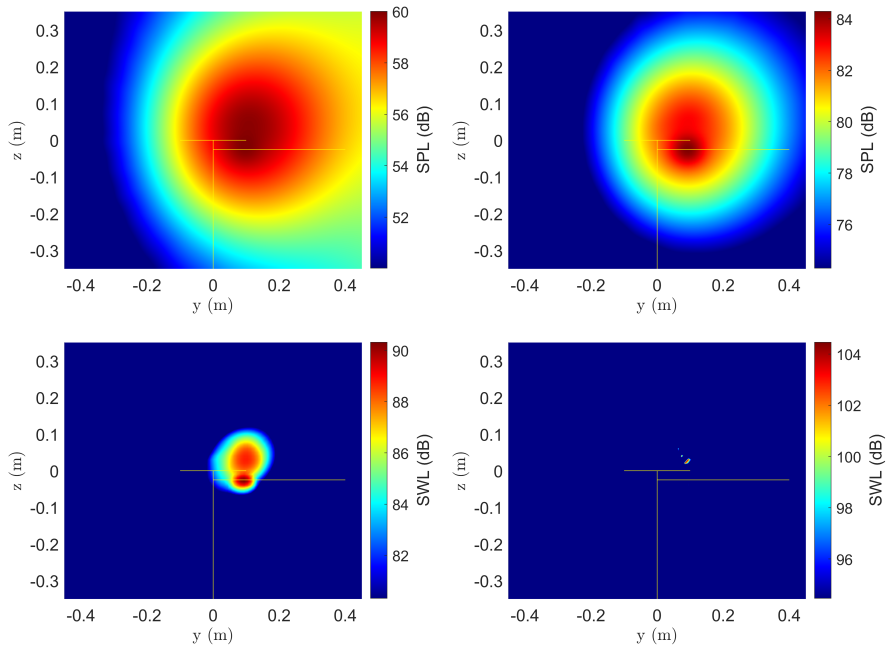

Fig. 4 Sound source maps obtained with CBF (top left), NF (top right), CIRA (bottom left) and CLEAN SC (bottom right) at $7000\ RPM$ **for the beam of diameter** $0,015\ m$ **at** $-0,025\ m$ **and BPF harmonics from** 2 **to** 35**.**

In the light of these results, CIRA algorithm with same maps calculation parameters (FFT, source plane grid) was chosen in the following to study this tonal noise while avoiding CLEAN-SC excessive cleaning of maps. Please note that similar source locations were found with CLEAN-SC algorithm even if not shown here.

B. Source localization for BPF harmonics

The noise generation mechanism leading to tonal noise increase associated to the presence of the beam is investigated in more details in this part.

1. Frequency effect

As previous measurements [6] evidenced two main BPF harmonics humps centered on $5 * BPF$ and $20 * BPF$, sound source localization were performed at these BPF harmonics in order to better assess their contribution. Results obtained for the same operating point (i.e. $7000\ RPM$ for the beam of diameter $0,015\ m$ at $-0,025\ m$) with CIRA are presented Fig. 5. To complement what has been seen in CIRA map Fig. 4 for BPF harmonics $2-35 * BPF$, the first hump seems to be linked to a source located just above the blade tip, and the second hump to a source just below the beam at similar span location. This might suggest two different noise source mechanisms.

The main source location obtained for the first BPF harmonics hump seems not consistent with the fact that previous numerical simulations [7, 8] suggested that the first hump BPF harmonics increase was mainly related to the beam radiation. However these simulations were performed on the same rotor but at a higher rotational speed, with a higher beam diameter and a smaller beam-rotor distance. The influence of these parameters on source maps is thus investigated in the following.

2. Parametric study

The effect of the rotor rotational speed on the rotor-beam tonal noise is first addressed for the same beam diameter ($0,015\ m$) and location ($-0,025\ m$). Sound power levels and locations respect to the rotor and the beam of the maximal source points identified on CIRA maps are compared in Fig. 6 for three rotational speeds ranging from 6000 to 8000 RPM. Please note that, for each case, the color of the marker corresponds to the SWL given in the colorbar, permitting to see both the evolution of the source position and its level. The location of the first hump stays just above the blade

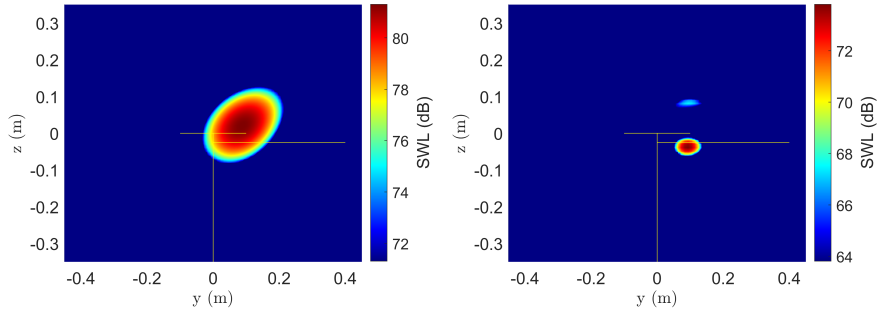

Fig. 5 Sound source maps obtained with CIRA at $7000\ RPM$ **for the beam of diameter** $0,015\ m$ **at** $-0,025\ m$ **and BPF harmonics** $5 * BPF$ **(left) and** $20 * BPF$ **(right).**

tip and the one of the second hump just below the beam for all rotational speeds, with an increase of the source SWL with the rotational speed (i.e. a change of color from blue to red of the markers corresponding to $5 \times BPF$) as already pointed out in previous experiments [6]. The source location associated to $5 * BPF$ harmonic moves slightly towards the blade tip with the rotational speed. It can be noticed that the average source locations identified by CIRA for all rotational speeds and BPF harmonics is located at 89% of the blade radius, which is consistent with previous numerical results obtained for the $0,02\ m$ beam at $-0,02\ m$ and 8000 RPM, which showed that the SPL distribution along the beam was maximal around $80-90\%$ of the blade radius for BPF harmonics $5 * BPF$, $7 * BPF$ and $9 * BPF$ [8].

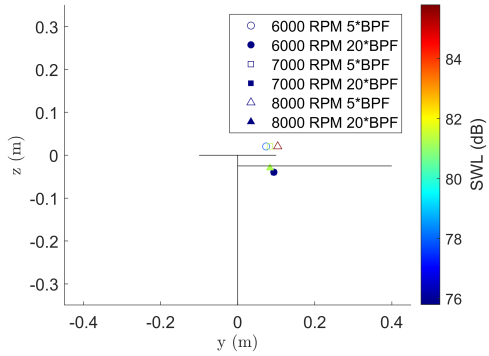

Fig. 6 Sound source levels and locations of source maps maximal obtained with CIRA for $5 * BPF$ **(empty markers) and** $20 * BPF$ **(filled markers) at** $6000\ RPM$ **(circles),** $7000\ RPM$ **(squares) and** 8000 **RPM (triangles) for the beam of diameter** $0,015\ m$ **at** $-0,025\ m$**.**

The effect of the rotor-beam distance is now assessed for the beam of diameter $0,015\ m$ and the intermediate rotational speed of 7000 RPM. Maximal source points locations ans SWL identified on source maps are reported Fig. 7 for distances between $-0,02\ m$ and $-0,03\ m$ (new beam locations are indicated by dashed lines). Similar source locations than previously are found for BPF harmonics of the two humps, with a decrease of the SWL when the rotor-beam distance increases consistent with previous experiments [6] for $5 * BPF$. Interestingly, the SWL of the source found for $20 * BPF$ varies with the rotor-beam distance (variation not visible in the figure because of the chosen color scale) with a maximal SWL of 73.8 dB at $-0.025\ m$, respect to 59.8 dB at $-0.02\ m$ and 72.5 dB at $-0.03\ m$. A similar evolution of the second hump level with the rotor-beam distance was already noticed in previous experiments for farfield spectra at an other rotational speed [6]. The average of source locations found for all rotor-beam distances remains on the same area with 87% of the blade radius.

The effect of the beam diameter is finally assessed for the intermediate rotor-beam distance of $-0,025\ m$ and rotational speed of 7000 RPM. Fig. 8 shows the locations and SWL of maps maximal points for cylindrical beams with diameters ranging from $0,01\ m$ until to $0,02\ m$. The beam diameter seems to not affect source locations associated to the two BPF harmonics humps at this rotor-beam distance and rotational speed, whereas the source SWL increases with the beam diameter for $5 * BPF$ as already shown [6]. As for the rotor-beam distance, the SWL evolution of the source

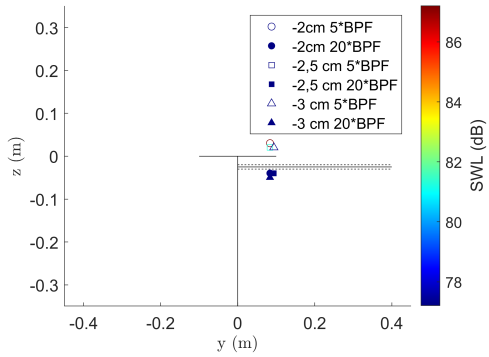

Fig. 7 Sound source levels and locations of source maps maximal obtained with CIRA for $5 * BPF$ (empty markers) and $20 * BPF$ (filled markers) for the beam of diameter $0,015$ m at -0.02 m (circles), -0.025 m (squares) and -0.03 m (triangles) from the rotor disk plane, at 7000 RPM.

found for $20 * BPF$ follows a different trend with a maximal SWL of 73.8 dB for the beam diameter of 0.015 m, respect to 70 dB for 0.01 m and 71.2 dB for 0.02 m. A similar evolution of the second hump level with the beam diameter was already noticed in previous experiments for farfield spectra at an other rotor-beam distance [6]. Sources remain located at 89% of the blade radius in average.

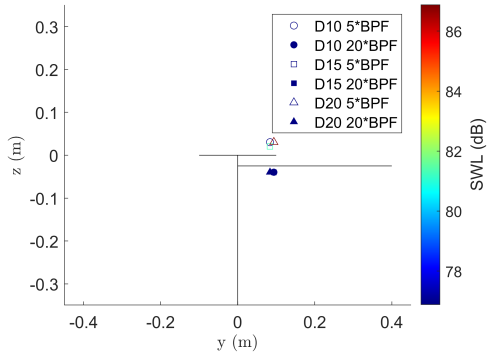

Fig. 8 Sound source levels and locations of source maps maximal obtained with CIRA for $5 * BPF$ (empty markers) and $20 * BPF$ (filled markers) for the beam of diameters $0,01$ m (circles), 0.015 m (squares) and -0.02 m (triangles) at 0.025 m from the rotor disk plane and 7000 RPM.

3. Noisier configuration

Previous numerical simulations done for the noisier configuration, corresponding to the maximal rotational speed of 8000 RPM, the beam of maximal diameter $0,02$ m located at the minimal distance from the rotor disk plane of $0,02$ m, showed that the beam was the main contributor to the farfield radiated noise for BPF harmonics of the first hump [7]. Microphone array measurements have been thus also done on this rotor-beam configuration to allow source localization at $5 * BPF$, which is supposed to be associated to the beam, and at $20 * BPF$ which was not studied in previous numerical simulations due to a lack of resolution. Source locations and SWL obtained in this configuration are presented Fig. 9. Contrary to previous configurations, sources corresponding to the two BPF harmonics humps are both located near the blade tip. To confirm those results, source maps integrated on several harmonics of each hump, $3-7 * BPF$ and $18-22 * BPF$, were also computed, leading to similar source locations. To go further, measurements were additionally performed with the beam in the opposite direction, meaning that the blade goes away from the array when passing above the beam. Those results are added on the left part of Fig. 9, showing that sources associated to $5 * BPF$ and $20 * BPF$ are in this case both located near the beam but slightly closer to the rotor axis (average source locations of 81% of the blade radius instead of 94% of the blade radius with beam on the right side).

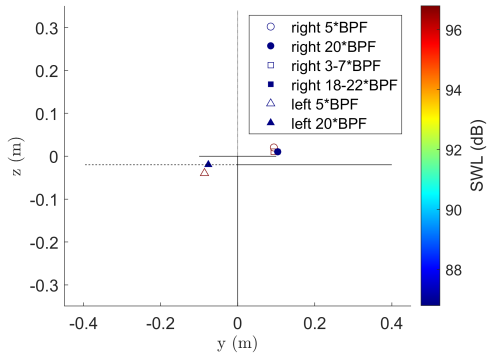

Fig. 9 Sound source levels and locations of source maps maximal obtained with CIRA for $5 * BPF$ (empty markers) and $20 * BPF$ (filled markers) for the beam of diameter $0,02\ m$ at $0.02\ m$ from the rotor disk plane on the right side (circles) and left side (triangles) at 8000 RPM. Results obtained for the right side and integrated over $3-7 * BPF$ and $18-22 * BPF$ harmonics (squares) are also indicated.

To complete these observations, spectra measured by the directivity antenna at a latitude angle of $-40°$ for both beam locations are compared Fig. 10, as well as the global directivity for $5 * BPF$. An asymmetry is seen on both graphs, leading to lower BPF harmonics SPLs with the beam on the left side (blades going away from the microphones when passing above the beam) and almost an opposite directivity. As it is expected that the part of the setup which is the main contributor to farfield levels is the same for both beam locations, this difference in vertical position of sources may be explained by a curvature of the wave fronts that may not be spherical as in the monopolar source model used by the beamforming process [9]. As we know that, for this noisier configuration, the noise source at $5 * BPF$ is supposed to be associated with beam radiation due to unsteady loading, a precise analyse of the wave fronts seems necessary. This is what is done in the next section.

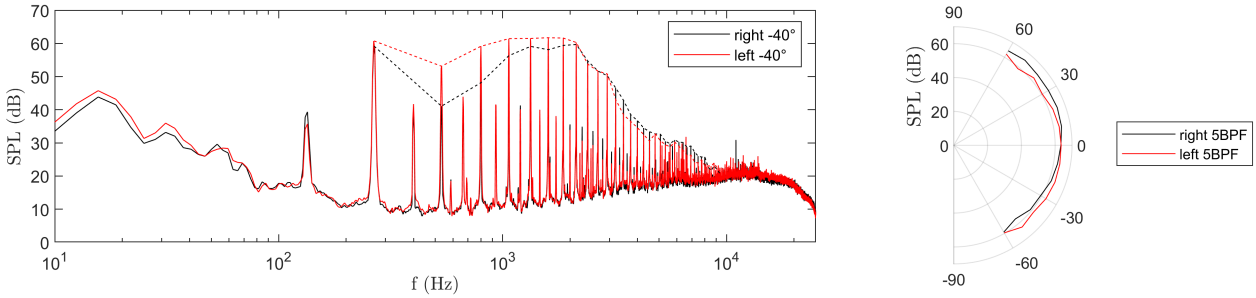

Fig. 10 Sound pressure levels (SPL) at -40 (left) and directivity at $5 * BPF$ (right) measured by directivity antenna at $8000\ RPM$ for the beam of diameter $0.02\ m$ at $-0.02\ m$ located on the left and right side.

V. Numerical insights

In order to be able to better understand sound source localization results obtained on the noisier simulated rotor-beam configuration compared to numerical ones [7, 8], additional simulations were performed to complete the study.

A. Numerical setup

The experimental configuration was simulated with the computational fluid dynamics (CFD) commercial software Fluent v2020 R1. The computational domain is split into two meshes: a rotating inner mesh including the rotor and the upper part of the hub, and a static outer mesh including the beam, a main part of the hub and all far-field boundary conditions. Interfaces, represented by black lines in Figure 11(right), are created for the communication between the two meshes. The total number of cells is around 7 millions. Each volume is meshed with polyhedral cells, and prism

layers are generated for the discretization of the boundary layer on none-slip walls. The thickness of the first prism layer is calculated to target a $Y+$ value around 1. The surface mesh for the rotor, beam and hub walls and a split of the volume mesh are shown Figure 11. The upstream, lateral and downstream boundaries in the outer volume are modeled as pressure inlet, slip wall and pressure outlet respectively. The rotor, beam and hub walls are modeled by none-slip walls.

Since the maximal Mach number at the blade tip is around 0.3, the flow can be assumed incompressible, and a segregated solver with a constant density is selected. As the local Reynolds number (based on the local velocity and the chord length) increases from 25.000 at the blade root to 130.000 at the blade tip, the boundary layers are mainly laminar, and a fully turbulent URANS model is not appropriate in that case. To solve directly the Navier-Stokes equations without turbulence or subgrid scale model, the implicit large eddy simulation (iLES) model is chosen, but only the largest turbulent structures are solved. Second order schemes are chosen for the spatial and temporal discretizations, and the time-step in the implicit unsteady solver is set to obtain a complete rotation of the rotor mesh every 400 time-steps.

To propagate the pressure fluctuations from none-slip-wall surfaces to the farfield, a Ffowcs-Williams and Hawkings (FW-H) analogy is used. The computed SPL were compared to farfield acoustic measurements for validation in previous studies [7, 8].

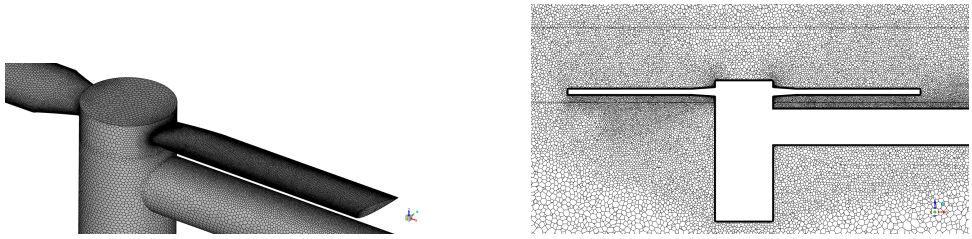

Fig. 11 Rotor, beam and and hub surface mesh (left), and cut of volume mesh (right)

B. Sound pressure calculation

FW-H analogy has been used to obtain sound pressure signals in the farfield from beam, rotor, and hub aerodynamic surface fluctuations. The resulting sound pressure signals are obtained at a sampling frequency of 53333 Hz during 0.1116 s. Numerical spectra can be then computed by applying the fast Fourier transform (FFT) to those signals with a Hanning window applied on 1 segment, leading to a frequency resolution of 9 Hz.

This post processing was validated previously against measurements for farfield radiation towards the directivity antenna [7, 8]. As the microphone array is not in the farfield on the whole frequency range, to complete this validation a comparison of SPL spectrum obtained numerically at the nearfield microphone location with the measured one is presented Figure 12. This shows that, even at this location that is not in the farfield for the whole frequency range, the sound pressure assessment is good. In particular, tonal noise is correctly assessed by numerical simulations until the harmonic $12 * BPF$, which allows to perform analysis on the first BPF hump.

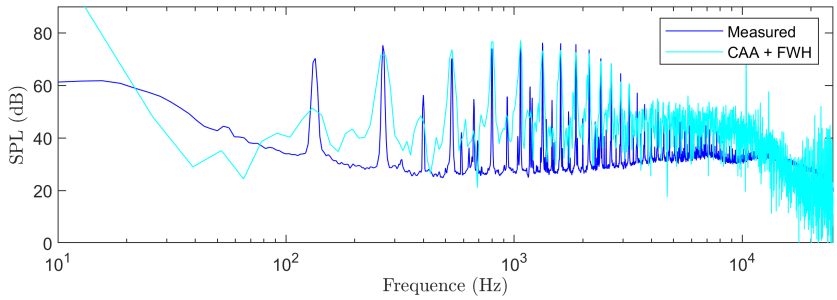

Fig. 12 Nearfield microphone sound pressure levels (SPL) measured and obtained by numerical simulations.

C. Wave fronts

In order to better understand noise source maps, FW-H analogy is used to obtain the sound pressure on 2 perpendicular square planes positioned between the rotor and the array. This calculation is done in a horizontal plane defined by 1024 points located at $x = [0,2 : 0,015 : 0,7]$ m and $y = [-0,25 : 0,015 : 0,25]$ m, and in a vertical plane also defined by 1024 points located at same x-axis locations and at $z = [-0,25 : 0,015 : 0,25]$ m. Because of the different distances between the rotor and the calculation points, sound pressure signals have not the same time axis. Thus an interpolation is done on the time range which is common to the different signals to obtain wave fronts at each time step. Examples of horizontal and vertical wave fronts filtered on the frequency range $1 - 12 * BPF$ are presented Figure 13. The microphone array location is indicated by a black line on both planes. Wave fronts seem to be parallel to the main part of the array in both planes, however they were computed on the whole frequency range for which numerical simulations are able to retrieve experimental spectra.

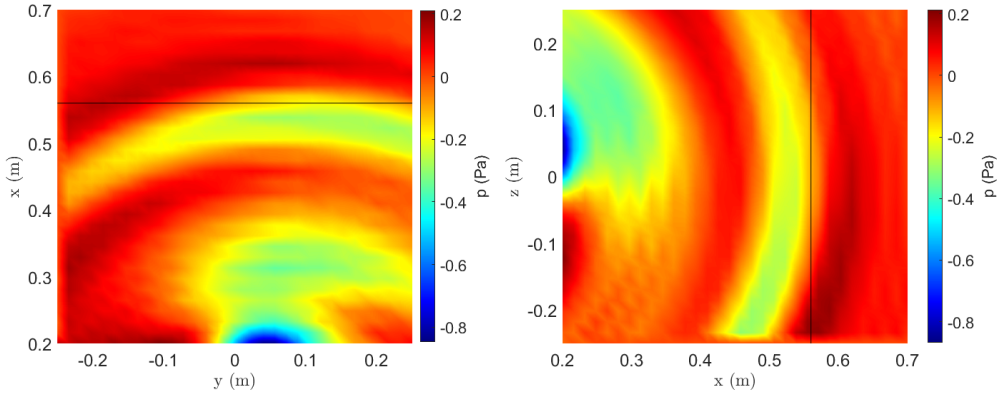

Fig. 13 Horizontal (left) and vertical (right) wavefronts between the source and the array planes obtained by numerical simulations for the $1 - 12 * BPF$ frequency range.

In order to investigate more accurately sound wave propagation between the rotor-beam configuration and the array, a band-pass filter is applied on the interpolated instantaneous sound pressure fields around $5 * BPF$. Corresponding wave fronts are presented Fig. 14. Resulting wave fronts are different from the ones obtained with a rotor alone (spiral shape [21]) which confirms that the interaction noise is dominant here. Those cleaner wave fronts allows to retrieve array focalization indicated by dotted lines. This focalization is consistent with source locations obtained at $5 * BPF$ for the same configuration by experimental source localization : $\sim 80\%$ of the blade radius in the positive y direction (beam side) and ~ 1 beam diameter above the rotor disk plane in the positive z direction.

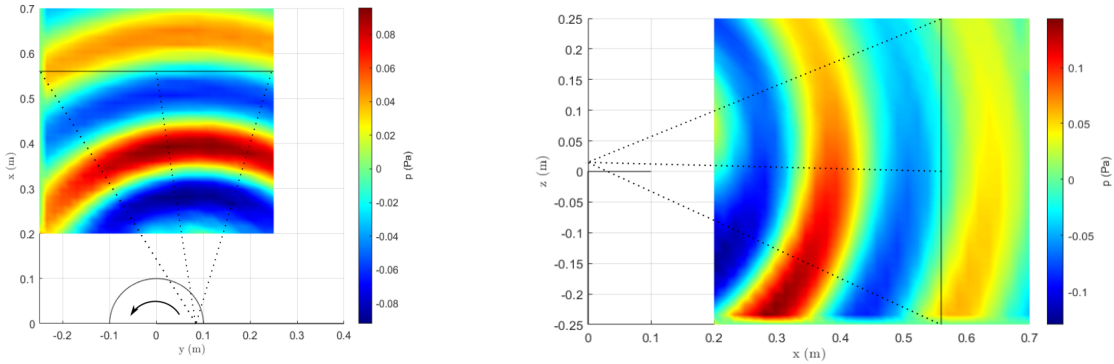

Fig. 14 Horizontal (left) and vertical (right) wavefronts between the source and the array planes obtained by numerical simulations at $5 * BPF$.

Same results were obtained for other instantaneous fields but a slight deviation can be observed on vertical wave fronts along time (see Fig. 15). This might be due to lack of aerodynamic stabilization before to compute sound pressure

signals using FW-H.

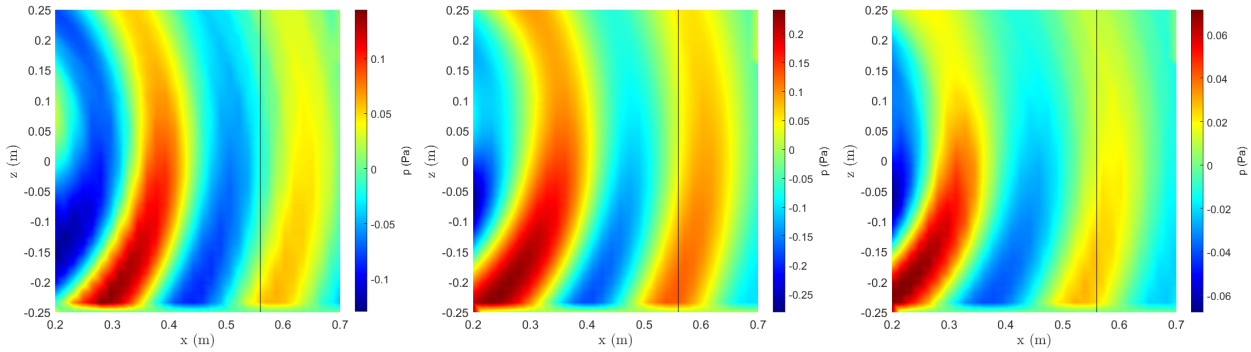

Fig. 15 Vertical wavefronts between the source and the array planes obtained by numerical simulations at $5 * BPF$ along time (from left to right).

D. Discussion

It is quite challenging for source localization to try to distinguish small scale rotor-beam interaction noise sources that may come from the rotor or the beam that are at $0,02\ m$ apart on this noisier configuration, especially for the low frequency range corresponding to first BPF harmonics. Source maps obtained in previous section from experiments indicate a source location for the first BPF harmonics hump that is not on the beam as expected from previous numerical studies [7, 8] and from recent analytical model developments [22], which showed that this noise component was associated to unsteady loading on the beam. It was also shown that the beam orientation respect to the array (rotor blades going towards or away from the array when passing above the beam) influence the location of the both humps sources, as well as the levels and the directivity of first BPF harmonics. However the $5 * BPF$ source location near the blade tip on maps can be explained by the particular wave fronts shape obtained by new iLES simulations associated to FW-H. This insight seems to indicate that for other experimental rotor-beam configurations (varying beam diameters, rotor-beam distances and rotational speeds), sources located near the blade tip on source maps seems to be related to beam radiation, whereas sources located at other places seems to be related to another rotor-beam interaction noise mechanism. This suggests also that for the noisier configuration the second hump increase is also due to beam unsteady loading as the corresponding source is located at the same place as the one of the first hump.

VI. Conclusions

Directivity measurements performed previously in anechoic room on a small-scale low Reynolds number two-bladed rotor of $0.2\ m$ diameter with NACA0012 blade profile in interaction with beams have shown that the overall source level of this setup increases with the beam diameter, the rotational speed and the reduction of rotor-beam distance. It was also shown that the presence of the beam increases harmonics of the blade passing frequency (BPF) leading to two humps on spectra, one centered around $5 * BPF$ and another centered around $20 * BPF$.

In this study several algorithms were used to perform sound source localization on fixed interaction noise sources of similar rotor-beam configurations with varying parameters: rotational speed, beam diameter and beam location respect to the rotor disk plane. Resulting source maps obtained for the two humps of BPF harmonics indicate in most cases sources located near the blade tip for the first hump and near the beam for second one at $\sim 85\%$ of the blade radius, with levels evolutions respect to the different parameters consistent with those measured by the farfield directivity antenna. For the noisier configuration with the biggest beam, closest to the rotor at the highest rotational speed, sources of both BPF harmonics humps are located near the blade tip. As this was not consistent with previous numerical simulation performed on the same configuration that showed that the unsteady loading on the beam was the main contributor to farfield radiation at $5 * BPF$, measurements with the beam on the opposite side (rotor blades going away from the array while passing above the beam) were also performed. In this case source locations of both humps are found near the beam on source maps, which seemed to indicate different wave fronts orientation for these two beam positions. This asymmetry was confirmed by the comparison of farfield spectra and directivity for the opposite beam positions.

Finally new numerical simulations were performed to allow Ffowcs-Williams and Hawkings analogy calculations on 1 horizontal and 1 vertical planes between the rotor-beam setup and the microphone array to assess wave fronts. Wave fronts shapes filtered around $5 * BPF$ indicate an array focalization that can explain source locations on maps, allowing to conclude which source locations can be associated to the beam radiation and which ones not.

To confirm those conclusions numerical simulations over a longer time period to obtain wave fronts with the beam on both sides successively could be performed. It is also envisaged to apply microphone array processing to numerical signals in order to verify that same source locations are obtained for the first BPF harmonics hump on source maps. This methodology would also allow to help the understanding of other rotor interaction noise mechanisms.

Acknowledgments

The authors gratefully acknowledge financial support from the French Defense Procurement Agency (DGA). They are grateful to ISAE-SUPAERO technical staff for their contribution to the experimental campaign.

References

[1] Brentner, K., and Farassat, F., "Helicopter noise prediction: The current status and future direction," J. Sound Vib., Vol. 170, No. 1, 1994, pp. 79–96.

[2] Zawodny, N., Boyd, D., and Burley, C., "Acoustic characterization and prediction of representative, small-scale rotary-wing unmanned aircraft system components," Proceedings of the American Helicopter Society (AHS) 72nd Annual Forum, May 16-19, 2016.

[3] Zawodny, N., and Boyd, J., D., "Investigation of rotorairframe interaction noise associated with small-scale rotary-wing unmanned aircraft systems," in Proceedings of the American Helicopter Society (AHS) 73rd Annual Forum, May 9-11, 2017.

[4] Wu, Y., Kingan, M., and Go, S., "Propeller-strut interaction tone noise," Physics of Fluids, Vol. 34, 2022.

[5] Roger, M., Vella, E., Rendon, J., Moreau, S., and Pereira, A., "Aerodynamic and Sound-Scattering Effects in Rotor-Strut Interaction Noise of Small-Size Drones," AIAA Aviation and Aeronautics Forum and Exposition, 2023.

[6] Gojon, R., Parisot-Dupuis, H., Mellot, B., and Jardin, T., "Aeroacoustic radiation of low Reynolds number rotors in interaction with beams," The Journal of the Acoustical Society of America, Vol. 154, 2023, pp. 1248–1260.

[7] Gojon, R., Doué, N., H., P.-D., B., M., and Jardin, T., "Aeroacoustic radiation of a low Reynolds number two-bladed rotor in interaction with a cylindrical beam," The 28th AIAA/CEAS Aeroacoustics 2022 Conference, 2022.

[8] Doué, N., Gojon, R., and Jardin, T., "Numerical investigation of the acoustics radiation of a two-bladed rotor in interaction with a beam," The 6th Symposium on Fluid-Structure-Sound Interactions and Control, 2023.

[9] Billinsgley, J., and Kinns, R., "The acoustic telescope," J. Sound Vib., Vol. 48, No. 4, 1976, pp. 485–510.

[10] Piet, J., and Elias, G., "Modélisation du champ acoustique incident sur la coiffe d'Ariane 5 par des sources simples," Office national d'études et de recherches aérospatiales, 1994.

[11] Brooks, T., and Humphreys, W., "A Deconvolution Approach for the Mapping of Acoustic Sources (DAMAS) Determined from Phased Microphone Arrays," J. Sound Vib., Vol. 294, No. 4, 2006, pp. 856–879.

[12] Sijtsma, P., "CLEAN based on spatial source coherence," Int. J. Aeroacoust., Vol. 6, No. 4, 2007, pp. 357–374.

[13] Antoni, J., "A bayesian approach to sound source reconstruction: Optimal basis, regularization, and focusing," The Journal of the Acoustical Society of America, Vol. 131, No. 4, 2012, pp. 2873–2890.

[14] Sijtsma, P., Oerlemans, S., and Holthusen, H., "Location of rotating sources by phased array measurements," In 7th AIAA/CEAS aeroacoustics conference and exhibit, 2001, p. 2167.

[15] Oerlemans, S., Location and quantification of helicopter noise sources in a wind tunnel, 2006.

[16] Sijtsma, P., "Feasibility of in-duct beamforming," In 13th AIAA/CEAS Aeroacoustics Conference, 2007, p. 3696.

[17] Oerlemans, S., Fisher, M., Maeder, T., and Kögler, K., "Reduction of wind turbine noise using optimized airfoils and trailing-edge serrations," AIAA journal, Vol. 47, No. 6, 2009, pp. 1470–1481.

[18] Zawodny, N., Pettingill, N., and Thurman, C., "Identification and Reduction of Interactional Noise of a Quadcopter in Hover and Forward Flight Conditions," In INTER-NOISE and NOISE-CON Congress and Conference Proceedings, Vol. 265, No. 5, 2022, pp. 2947–2958.

[19] Gojon, R., Jardin, T., and Parisot-Dupuis, H., "Experimental investigation of low Reynolds number rotor noise," The Journal of the Acoustical Society of America, Vol. 149, No. 6, 2021, pp. 3813–3829.

[20] Sijtsma, P., "CLEAN based on spatial source coherence," In the 13th AIAA/CEAS Aeroacoustics Conference, 2007, p. 3436.

[21] Horváth, C., Envia, E., and Podboy, G. G., "Limitations of phased array beamforming in open rotor noise source imaging," AIAA journal, 2014, pp. 1810–1817.

[22] Vella, E., R., G., Parisot-Dupuis, D. N., H., Jardin, T., and Roger, M., "Mutual Interaction Noise in Rotor-Beam Configuration," The 30th AIAA/CEAS Aeroacoustics 2024 Conference, 2024.